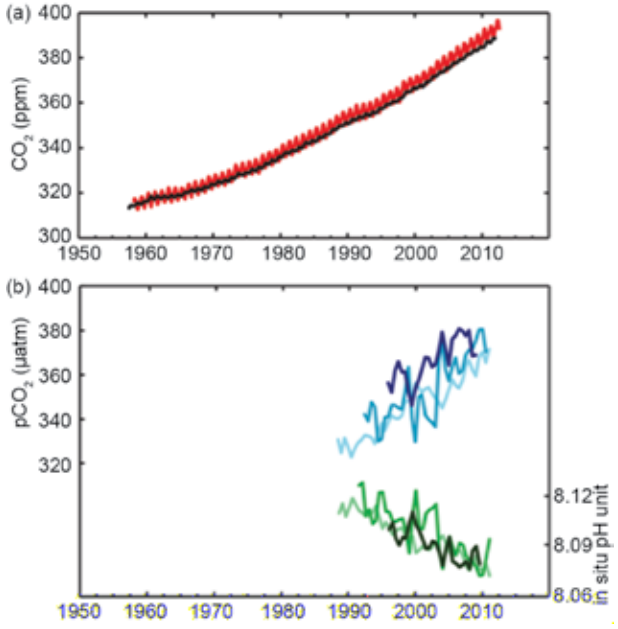

Fig. 3.38. Multiple observed indicators of a changing global carbon cycle: (a) atmospheric concentrations of carbon dioxide (CO_2) from Mauna Loa (19°32'N, 155°34'W; red) and South Pole (89°59'S, 24°48'W; black) since 1958. (b) Partial pressure of dissolved CO_2, at the ocean surface (blue curves) and in situ pH (green curves), a measure of the acidity of ocean water. Measurements are from three stations from the Atlantic (29°10'N, 15°30'W, dark blue/dark green; 31°40'N, 64°10'W, light blue/light green) and the Pacific Oceans (22°45'N, 158°00'W, blue/green) (Source: Alexander et al. 2013.)

Alaska showed a pH decline of −0.0017 yr^{-1} between 1991 and 2006, in agreement with observations at the HOT site (Byrne et al. 2010). This rate of pH change is also consistent with repeat transects of CO_2 and pH measurements in the western North Pacific (winter: −0.0018 ±0.0002 yr^{-1}; summer: −0.0013 ±0.0005 yr^{-1}; Midorikawa et al. 2010). The pH changes in Southern Ocean surface waters are less certain because of the paucity of long-term observations there, but pCO_2 measurements collected by ships-of-opportunity indicate similar rates of pH decrease there (Takahashi et al. 2009).

4) Global ocean phytoplankton—B. A. Franz, M. J. Behrenfeld, D. A. Siegel, and P. J. Werdell

Marine phytoplankton are responsible for roughly half the net primary production (NPP) on Earth, fixing atmospheric CO_2 into food that fuels global ocean ecosystems and drives the ocean's biogeochemical cycles. Phytoplankton growth is highly sensitive to variations in ocean physical properties, such as upper ocean stratification and light availability within this mixed layer. Satellite ocean color sensors, such as the Sea-viewing Wide Field-of-view Sensor (SeaWiFS; McClain 2009) and Moderate Resolution Imaging Spectroradiometer (MODIS; Esaias 1998), provide observations of sufficient frequency and geographic coverage to globally monitor physically-driven changes in phytoplankton distributions. In practice, ocean color sensors retrieve the spectral distribution of visible solar radiation reflected upward from beneath the ocean surface, which can then be related to changes in the photosynthetic phytoplankton pigment, chlorophyll-*a* (Chl*a*; measured in mg m^{-3}). Here, global Chl*a* data for 2013 are evaluated within the context of the 16-year continuous record provided through the combined observations of SeaWiFS (1997–2010) and MODIS on Aqua (MODISA; 2002–present). Ocean color measurements from the recently launched Visible and Infrared Imaging Radiometer Suite (VIIRS; 2011–present) are also considered, but results suggest that the temporal calibration of the VIIRS sensor is not yet sufficiently stable for quantitative global change studies. All MODISA (version 2013.1), SeaWiFS (version 2010.0), and VIIRS (version 2013.1) data presented here were produced by NASA using consistent Chl*a* algorithms.

Annual mean Chl*a* concentrations from MODISA were computed in 4.6 × 4.6 km^2 equal area bins (Campbell et al. 1995) and mapped to an equirectangular projection. The resultant average Chl*a* distribution for 2013 (Fig. 3.39) is consistent with the well-established, physically-driven distribution of

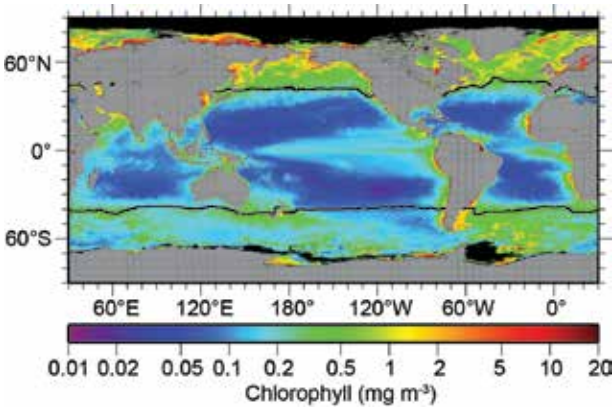

Fig. 3.39. Annual mean Chl*a* distribution (mg m^{-3}) derived from MODISA for 2013. Also shown is the location of the mean 15°C SST isotherm (black lines) delineating the boundary of the permanently stratified ocean (PSO). Chl*a* data are from the NASA Reprocessing of MODISA, version 2013.1. Data are averaged into geo-referenced equal area bins of approximately 4.6 × 4.6 km^2 (Campbell et al. 1995) and mapped to an equirectangular projection centered at 150°W.

nutrients (e.g., Siegel et al. 2013). Chl*a* values during 2013 ranged over three orders of magnitude, from <0.05 mg m^{-3} in the central ocean gyres to >50 mg m^{-3} in nutrient-rich coastal and subpolar waters. Global changes in Chl*a* during this past year were calculated for each geographic bin by subtracting monthly average values for 2013 from values during 2012, and then averaging the monthly anomaly fields to produce an annually-averaged distribution (Fig. 3.40a). Identical calculations were performed on MODISA SST (°C) data to produce an equivalent 2013 SST anomaly (Fig. 3.40b). Positive correlations and inverse correlations between these Chl*a* and SST anomalies are shown in Fig. 3.40c, following the graphical approach of O'Malley et al. (2010). Chlorophyll concentrations during 2013 were also compared to values for the full MODISA mission lifespan (Fig. 3.41). For this analysis, monthly climatological average Chl*a* values (2002–13) were subtracted from monthly values for each year to produce an anomaly time series.

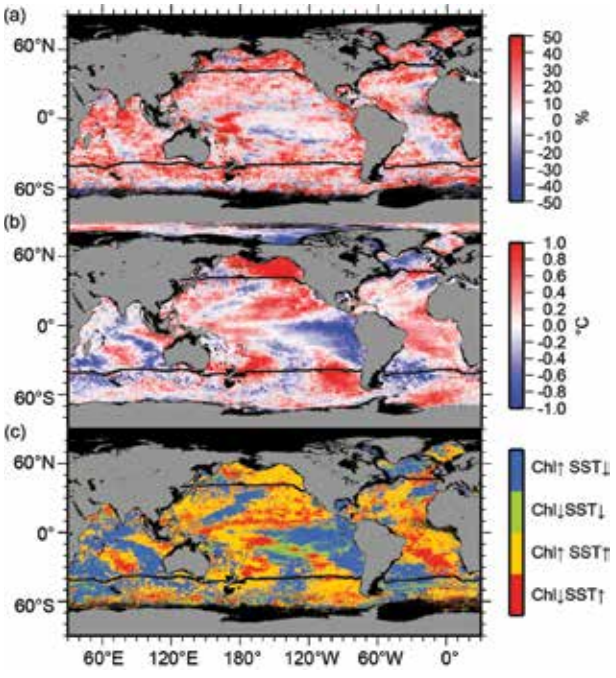

Fig.

In Figs. 3.39 and 3.40, black lines at approximately 40°N and 40°S delineate the relatively stable, permanently-stratified ocean (PSO) from higher-latitude systems, where strong seasonality in surface mixing, temperature, and sunlight drive strong annual plankton cycles. The PSO occupies ~74% of the global ocean surface area, maintains annual-average surface temperatures >15°C, and remains perpetually depleted in surface nutrients (Behrenfeld et al. 2006). Previous studies and annual *State of the Climate* assessments (e.g., Behrenfeld et al. 2006; O'Malley et al. 2010; Siegel et al. 2012) have demonstrated significant inverse correlations between chlorophyll and SST anomalies for the PSO. The expectation for these stratified waters is that a warming sea surface layer is associated with shallower mixing depths, reduced vertical nutrient transport, and higher average mixed layer light levels that together drive decreases in phytoplankton chlorophyll (Behrenfeld et al. 2006). Consistent with these earlier studies, the 2013 versus 2012 anomalies show that regions of decreasing SST (a proxy for stratification) (Fig. 3.40b) were associated with increasing Chl*a* (Fig. 3.40a). The predominance of this relationship is illustrated in Fig. 3.40c by the abundance of blue pixels relative to green. However, the surprising finding for 2013 was that the opposite relationship of decreasing Chl*a* with increasing SST was not equally prominent (i.e., red pixels do not clearly outnumber yellow pixels in Fig. 3.40c). In particular, regions of strong warming across the Pacific were often dominated by increases in Chl*a* (Fig. 3.40c). The reason for this discrepancy from previous years is not clear, but an issue with MODISA Chl*a* retrievals during the past two years cannot yet be ruled out. Regarding this latter possibility, it is noted that: (1) monthly average Chl*a* values during 2012 were at times lower than during the extreme 1998 El Niño year (Fig. 3.41a), yet surface ocean physical properties were not so anomalous during 2012 as in 1998, and (2) the rise in Chl*a* during 2013 (Fig. 3.41a) was expressed throughout almost the entirety of the global ocean (i.e., Fig. 3.40a is predominantly red), which is inconsistent with previous years, including the extreme 1998 event (Behrenfeld et al. 2001).

The multimission record of monthly mean Chl*a* for the PSO, starting with the SeaWiFS mission and extending into the MODISA and VIIRS eras (OBPG 2013), exhibits three primary features shown in Fig. 3.41a: (1) annual maxima in Chl*a* associated with Northern Hemisphere spring–summer phytoplankton blooms; (2) a general offset between MODISA and SeaWiFS data during their 2002 to 2010 overlap

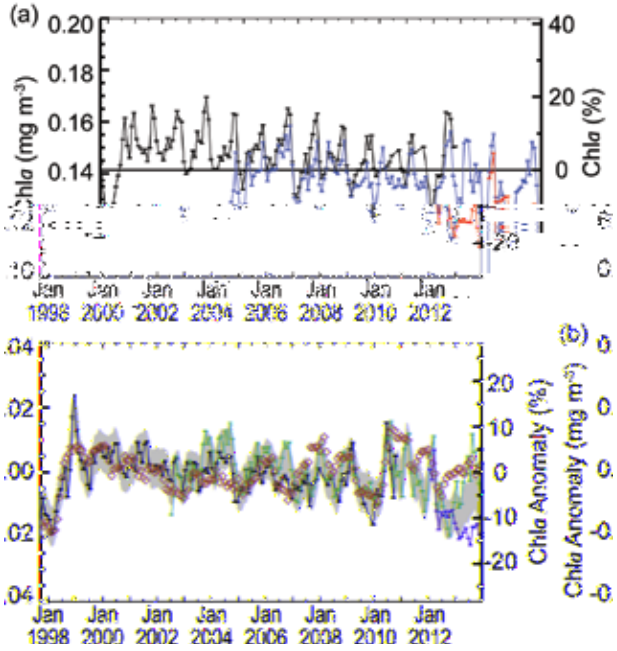

Fig. 3.41. Sixteen-year, multimission record of Chl*a* [mg m^{-3} (left) and % (right)] averaged over the PSO for SeaWiFS (black), MODISA (blue), and VIIRS (red): (a) Independent record from each mission, with horizontal black line indicating the multi-mission mean Chl*a* concentration for the region, and (b) monthly anomaly after subtraction of the monthly climatological mean (SeaWiFS relative to SeaWiFS climatology, MODISA and VIIRS relative to MODISA climatology). The gray region in (b) shows the averaged difference between SeaWiFS and MODISA over the common mission lifetime. Green diamonds show the multivariate ENSO index, inverted and scaled to match the range of the Chl*a* anomalies.

period; and (3) a strong divergence between MODISA and VIIRS Chl*a* for 2013. Regarding the latter feature, the trend in the VIIRS record through 2013 is flat or declining and remains near a historic low. This inconsistent behavior is believed to be due to temporal changes in radiometric performance of the VIIRS instrument that are currently being assessed.

With respect to SeaWiFS and MODISA data, the offset between sensors is essentially eliminated in the time series of Chl*a* monthly anomalies (Fig. 3.41b). Also shown in Fig. 3.41b is the multivariate ENSO index (MEI; Wolter and Timlin 1998), which generally tracks large-scale temporal variability in the monthly mean PSO Chl*a* record (Behrenfeld et al. 2006; Franz et al. 2013). Over the 16-year time series, Chl*a* concentrations in the PSO have varied by ±15% around a long-term mean of approximately 0.14 mg m^{-3}, with largest variations generally associated with El Niño to La Niña climatic events. Mean Chl*a* concentrations in the PSO trended upward from late 2012 to October 2013, for a total increase of approximately 10%, and then declined during the last few months of 2013. This range of variability in MODISA Chl*a* is within the envelope of the long-term record, and the directional character of the trends is consistent with expectations based on the change in MEI, but as previously discussed the magnitude of the change between 2012 and 2013 may not be accurately quantified in the current satellite record. The trend in VIIRS data for 2013, on the other hand, is entirely inconsistent with MEI changes thus adding support for the conclusion that VIIRS trends in 2013 are dominated by instrumental error (Fig. 3.41b). These errors and uncertainties in the 2012 and 2013 ocean color records from MODISA and VIIRS can potentially be reduced as more calibration data are collected and instrument radiometric degradation models are improved, but the results illustrate the caution that must be taken when interpreting ocean color measurements that are so highly sensitive to instrument calibration and characterization accuracy (Siegel and Franz 2010).

Caution is also warranted in the interpretation of satellite-observed temporal trends in Chl*a* concentration as indicators of climate-driven changes in phytoplankton net primary production (Behrenfeld et al. 2008; Siegel et al. 2013). Phytoplankton adjust their cellular chlorophyll content in response to environmental changes in light and nutrient availability, and this physiological response can contribute an order of magnitude variability in Chl*a* that can dominate monthly to interannual variations in PSO anomalies. As such, changes in the satellite time series can either reflect physiological variability or changes in abundance, with these two sources of variability having strongly divergent implications on NPP. Interpretation of the Chl*a* record is also complicated by limitations in the ability to separate optical signals of phytoplankton abundance from colored dissolved organic matter, which is simply assumed to co-vary in the traditional band-ratio algorithms employed here (e.g., Siegel et al. 2013).